2016 IEEE/RSJ International Conference on Intelligent Robots and Systems (IROS)
Daejeon Convention Center
October 9-14, 2016, Daejeon, Korea

System Design and Development of a Robotic Device for Automated Venipuncture and Diagnostic Blood Cell Analysis

Max L. Balter[1], Alvin I. Chen[1], Alex Fromholtz[1], Alex Gorshkov[1], Tim J. Maguire[2], and Martin L. Yarmush[3]

***Abstract*— Diagnostic blood testing is the most prevalent medical procedure performed in the world and forms the cornerstone of modern health care delivery. Yet blood tests are still predominantly carried out in centralized labs using large-volume samples acquired by manual venipuncture, and no end-to-end solution from blood draw to sample analysis exists today. Our group is developing a platform device that merges robotic phlebotomy with automated diagnostics to rapidly deliver patient information at the site of the blood draw. The system couples an image-guided venipuncture robot, designed to address the challenges of routine venous access, with a centrifuge-based blood analyzer to obtain quantitative measurements of hematology. In this paper, we first present the system design and architecture of the integrated device. We then perform a series of *in vitro* experiments to evaluate the cannulation accuracy of the system on blood vessel phantoms. Next, we assess the effects of vessel diameter, needle gauge, flow rate, and viscosity on the rate of sample collection. Finally, we demonstrate proof-of-concept of a white cell assay on the blood analyzer using *in vitro* human samples spiked with fluorescently labeled microbeads.**

I. Introduction

Blood testing is the most ubiquitous clinical procedure in the world, and accounts for 90% of diagnostic procedures administered in ambulatory and emergency care settings [1]. However, blood draw success rates depend heavily on clinician skill and patient physiology, and results are generated almost exclusively in centralized labs from large-volume blood samples using labor-intensive analytical techniques [2].

Traditionally, samples are drawn manually by venipuncture, analyzed in a centralized lab, and then results are returned to the medical staff to guide the intervention. This is a highly segmented process that involves specialized staff and facilities. Unexpected delays can arise due to difficulties in performing the venipuncture and from inefficiencies during the transport and subsequent analysis of the blood sample. Delays are particularly common in difficult patients, such as children, elderly, chronically-ill and obese populations, where small and fragile vessels or high levels of body fat may reduce the visibility of veins or make them more difficult to accurately puncture.

The accuracy and turnaround time of blood testing is especially important in time critical settings such as the emergency department (ED). Of the 350M tests performed in U.S. EDs each year, 25% are given urgent priority, indicating a turnaround time of 30–60 min, and 15% are given emergent priority, indicating a turnaround time of 15–30 min [3]. In these situations, failing to recognize the onset of critical conditions may have harmful consequences. Hence, there is a need for a device that can rapidly withdraw blood and run diagnostic analyses, particularly in emergency care settings.

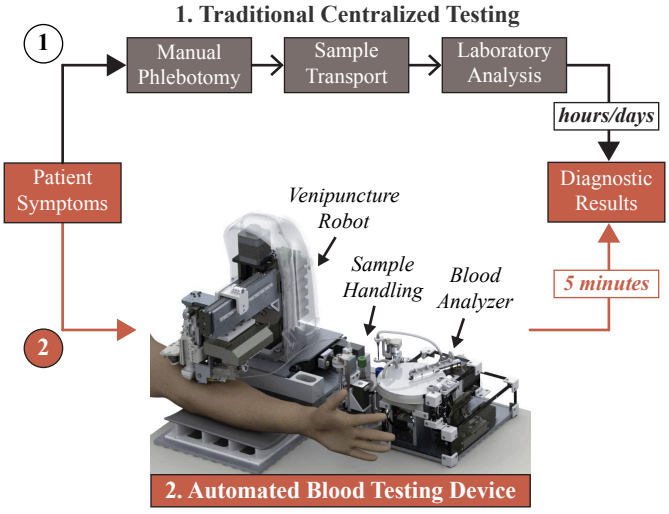

Fig. 1. Automated blood testing device that collects and analyzes the sample at the point-of-care. The technology is designed to replace the standard manual phlebotomy and central lab testing process (1-top). Instead, the device automatically draws blood and provides quantitative measurements of hematology within 5 minutes (2-bottom). The system combines a robotic venipuncture device, sample handling module, and blood analyzer unit.

Point-of-care (POC) devices have emerged as a potential solution to reduce turnaround times and expedite the clinical decision making process [4]. However, while POC devices have been adopted commercially, they are used for less than 10% of all blood tests for several reasons [5]. Firstly, virtually all of these devices rely on capillary blood from finger-pricks, which has been shown to provide less reliable measurements on large biomolecules compared to venous samples [6]. Moreover, such devices often require manual sample preparation and, on some tests, provide measurements with limited sensitivity and dynamic range compared to bench-top analyzers.

Lab automation systems have been developed to improve efficiency and reduce human error within centralized facilities [7]. Such systems include automated tube handling devices (e.g. AutoMate 2500 from Beckman Coulter), robotic pipetting instruments (e.g. Precision XS from BioTek), and

[1]M.L. Balter, A.I. Chen, A. Fromholtz, and A. Gorshkov are with the Department of Biomedical Engineering, Rutgers University, Piscataway, NJ, USA (corresponding author max.balter@rutgers.edu)
[2]T.J. Maguire is the Chief Executive Officer of VascuLogic, LLC, Piscataway, NJ, USA
[3]M.L. Yarmush is the Paul and Mary Monroe Distinguished Professor of Science and Engineering at Rutgers University

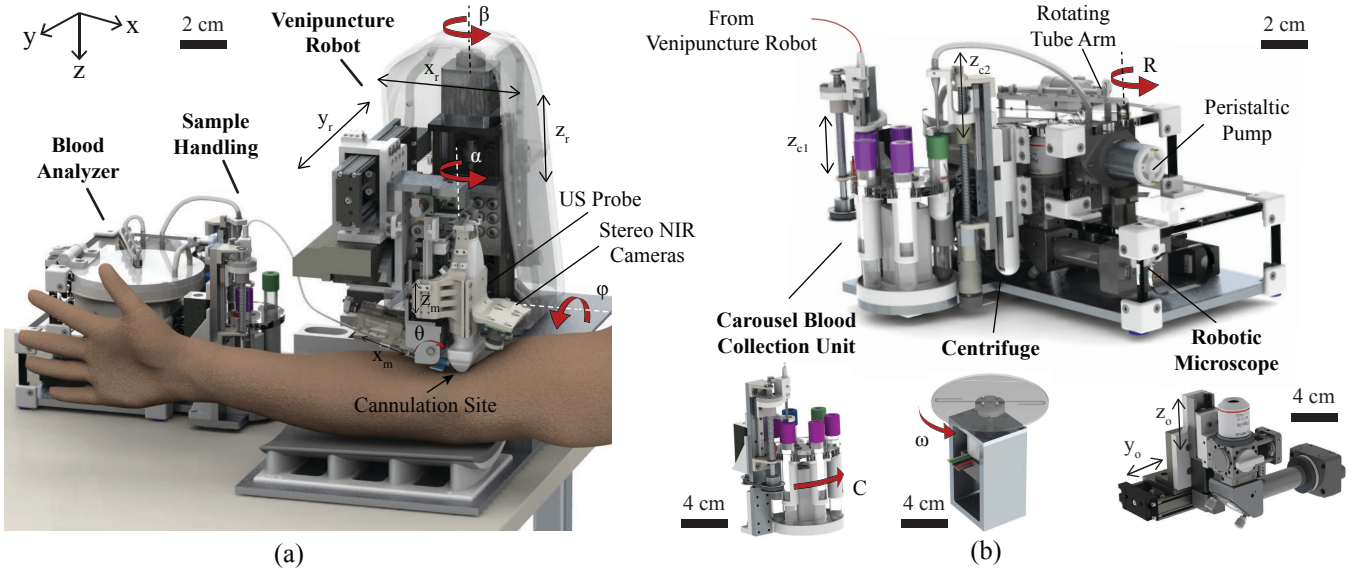

Fig. 2. (a) CAD rendering of the blood draw and analysis device. (b) Design of the sample handling module integrated with the blood analyzer unit.

automated hematology analyzers (e.g. XP-300 from Sysmex). Additionally, total lab automation systems exist that combine tube handling, sample preparation, and analysis units to fully automate diagnostic testing (e.g. XN-9000 from Sysmex). However, these systems are large, expensive, and decoupled from the blood sampling process, thus limiting their applicability in POC settings.

Despite recent progress in robotics, automation, and *in vitro* diagnostics, clinical adoption of these technologies has remained limited, and no end-to-end solution for complete POC testing exists today. To address this, our group is developing a platform device that enables complete end-to-end testing by performing blood draws and providing diagnostic results in a fully automated fashion (Fig. 1). By significantly reducing turnaround times, the device also has the capacity to expedite hospital work-flow, allowing practitioners to devote more time to treating patients. As a result of the improved work-flow, costs due to delays and complications may potentially be reduced.

A. Device Overview

The system couples an image-guided venipuncture robot, to address the challenges of routine venous access with a centrifugal microfluidic platform that performs the diagnostic analysis. The device is segmented into three distinct sub-systems—a robotic venipuncture device, automated sample handling module, and centrifuge-based optical blood analyzer unit (Fig. 2a).

The venipuncture device uses a combination of 3-D near-infrared (NIR) and ultrasound (US) imaging to localize blood vessels under the skin, and a robotic manipulator that orients and inserts the needle into the indicated vessel based on real-time image analysis and force feedback [8]–[10]. The blood sample is then extracted and transferred to the analysis unit, which provides blood measurements on sample volumes of $\sim$200 μl in approximately 5 minutes. In the current iteration of the device, the system performs two of the most commonly requested blood assays—an absolute white cell count and hematocrit measurement [11]—using centrifugal microfluidics and optical detection. High or low values beyond normal ranges can indicate the presence and condition of diseases or immunity.

In this paper, we describe the robotic integration of the venipuncture device, automated sample handling module, and blood analyzer unit (Sec. II). We then present preliminary results assessing the functional performance of each major sub-system (Sec. III). Collectively, these results serve as proof-of-concept for future studies evaluating the integrated platform in humans. Original contributions include: (1) a high-level description of the system design of the integrated device; (2) phantom cannulation testing on the venipuncture robot with the US probe oriented transversely for enhanced vessel visualization; (3) evaluation of pumping efficiency in the sample handling module; and (4) blood analysis on a simulated white cell assay.

II. System Design

The device consists of a venipuncture robot, sample handling module, and blood analyzer unit. Fig. 2b highlights the main components in the diagnostic unit. Currently, the system runs on a laptop computer (i7-4710HQ 2.5 GHz CPU), where the image processing is accelerated on an embedded GPU (Nvidia Quadro K2200M). The control software is written in LabVIEW, which monitors the execution and completion of each task and displays the diagnostic results.

A. Venipuncture Robot

Our group has developed a robotic venipuncture device to improve needle insertion success rates in difficult patients such as pediatric, geriatric, and obese populations. The robot uses NIR and US imaging to visualize veins, and a series of image analysis steps to enhance, segment, and reconstruct the

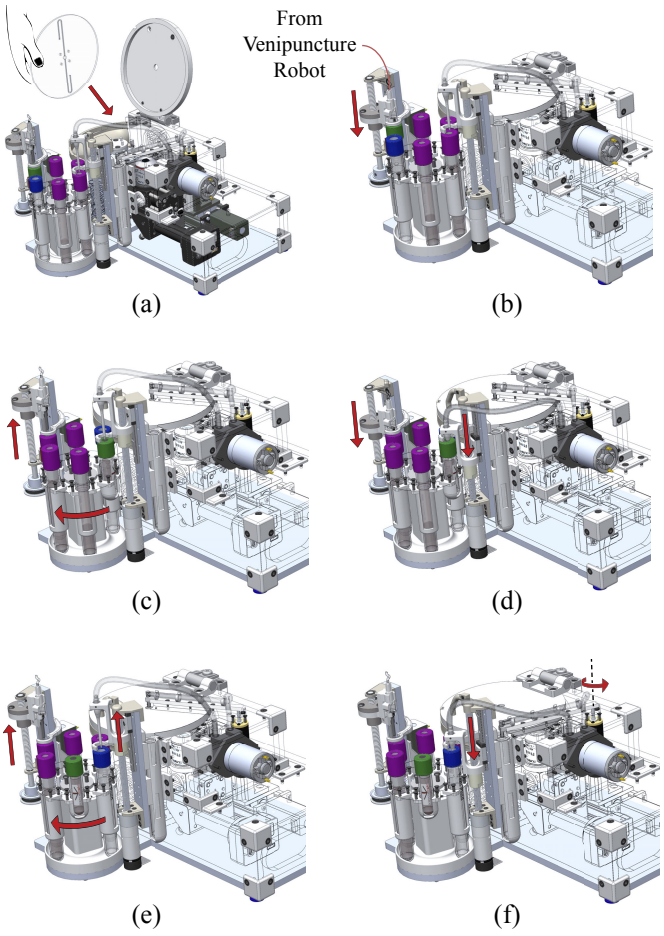

Fig. 3. Process flow of the sample handling module. (a) The clinician loads the microfluidic chip into the analyzer, and closes the lid. (b) Once the venipuncture device cannulates a vessel, the z_{c1}-stage lowers the back-end of the needle into the sample collection vial, rapidly filling the tube with blood. (c) The z_{c1}-stage rises and the carousel rotates 60°. At this point, steps a and b are repeated until the green-labeled vial is positioned under the pipette tip (green vial designated for use with our analyzer). (d) The z_{c2}-stage lowers the pipette tip into the green vial, and the peristaltic pump delivers the sample to the microfluidic chip. (e) Both the z_{c1} and z_{c2}-stage rise, and the carousel rotates 60°. (f) The back-end of the pump tubing rotates over to the waste container, the z_{c2} stage lowers into the saline solution vial stored in the carousel, and wash fluid is pumped through the tubing and into the waste bin.

vessels in 3-D. An optimal injection site is then selected by the clinician and tracked in real-time to continuously update the vessel position. Finally, the 3-D spatial coordinate is sent to the robot, which introduces the needle into the center of the vessel under US image and force guidance.

The design of the robot has been previously described in [10]. Briefly, the device consists of a 6-DOF base positioning system made up of three prismatic and revolute joints. The prismatic joints form a Cartesian gantry (x_r, y_r, z_r) whereas the revolute joints (α, ϕ, and β) align the end-effector with the vessel orientation. Contained within the end-effector is a pair of calibrated stereoscopic cameras (VRmMS-12, VRmagic), an 18 MHz US probe (L1830, Telemed), and a 3-DOF motorized needle manipulator.

Once oriented along the vein, the needle manipulator is used to guide the cannula into the center of the vessel. The manipulator is capable of adjusting the needle position and orientation in real-time based on image and force information provided to the robot. As seen in Fig. 2a, a micro linear stage (z_m) is used to adjust the height of the needle, a worm gear mechanism sets the insertion angle (θ), and a linear spindle drive controls the needle insertion (x_m). With this configuration, the manipulator can cannulate vessels from 1–6 mm below the skin while varying the insertion angle between 15–30° at each height.

1) Image Guidance: Stereo cameras, oriented in an eye-in-hand configuration on the manipulator, are used to create a 3-D map of the veins. The arm surface is segmented using an active contours technique, while vessels are segmented using a second-order match filtering approach, modeling veins as tube-like structures. After the clinician selects a cannulation site, the robot servos the US probe over to the indicated target vessel which is tracked in real-time using optical flow. Once positioned over the site, the US probe scans the target, providing a magnified view of the vessel. An active contours-based approach is implemented to segment and localize the center of the target vessel. Finally, position-based visual servoing is used for US-guidance in which the initial needle tip position is extracted from the robot kinematics and then tracked using optical flow along with the vessel center.

2) Force Sensing: During the procedure, insertion forces are monitored normal to the needle tip along one-axis (sensor resolution: 0.01 N; max load: 5 N). Analog force signals are digitized by a 12-bit A/D converter and transmitted to the host processor for real-time detection (i.e. 10 ms update rate). Peaks in the force profile can be observed when the needle punctures the skin (∼0.25 N) and subsequently the vein (∼1 N), indicating a successful venipuncture. At this point, the robot halts the needle insertion to prevent puncturing through the back of the vessel. In this fashion, the force sensor serves a critical safety function in the device. If, however, a fault is detected (e.g. excessive arm motion), the robot can release the needle into a sharps container via an electromagnet built into the manipulator. Studies have shown that off-axis forces are negligible, and thus can be ignored for the sake of reducing complexity in the needle manipulator [12].

B. Sample Handling Module

The sample handling module consists of a two-step approach to deliver the sample to the blood analyzer, as outlined in Fig. 3. The first phase utilizes a blood collection carousel to transfer the sample from the venipuncture robot to standard blood vials, and the second phase uses a peristaltic pump to then deliver the sample to the analyzer unit.

1) Blood Collection Carousel: Here, the blood draw is controlled via vacuum pressure contained in standard Vactuainer tubes interfacing with blood collection sets. Before the procedure, the clinician first loads the chip in the analyzer unit (Fig. 3a). After the needle insertion, a linear stage (denoted as z_{c1} in Fig. 2) connects the back-end of the needle to a blood collection vial (Fig. 3b). This causes the needle to pierce the rubber stopper on the Vactuainer tube,

breaking the vacuum and allowing blood to rapidly flow into the vial. Once 4 ml of blood is collected (as confirmed by a compact 780 nm laser diode and photodetector), the z_{c1}-stage rises and the carousel rotates to the next vial (Fig. 3c). This process repeats until the requested number of tubes have been filled (Fig. 3b–c), at which point the needle is withdrawn from the patient. In total, there are six slots in the carousel—four for standard blood vials (purple caps), one for a custom vial designed for use with our blood analyzer (green cap), and one for a saline wash fluid (blue cap) to clean the peristaltic pump between uses. The standard blood vials are included to allow sample collection for traditional laboratory analysis in addition to on-board measurements by the analyzer.

The carousel (C) and lead screw (z_{c1}) are actuated via bipolar stepper motors and controllers capable of high-resolution micro-stepping (0.028125°/step). The rotary carousel motion utilizes a direct drive mechanism to connect the motor axle with the blood vial cartridge, whereas the lead screw uses a pulley system to translate the glide nut.

2) Peristaltic Fluid Delivery: The sample then gets delivered to the analyzer unit via a peristaltic pump. Here, a linear spindle drive (z_{c2}) lowers a metal pipette tip into the green-capped blood vial, the pump is activated, and approximately 200 μl of sample is aspirated (Fig. 3d). The other end of the tubing is attached to a motorized rotating arm (denoted as R in Fig. 2) that positions the outlet over the microfluidic chip. Once the sample is delivered, the z_{c1} and z_{c2} stages rise, and the carousel rotates 60° to align the wash container with the metal pipette (Fig. 3e). The tubing outlet then rotates over to the waste container on the side of the device, the z_{c2} stage lowers into the saline solution vial, and wash fluid is pumped through the tubing to clean the system (Fig. 3f). The spindle drive and rotating tube arm are actuated via DC-brushed motors and position controllers (EPOS, Maxon Motors). Conversely, the DC-brushed motor driving the peristaltic pump is controlled using a transistor circuit and timing conditions in the software, resulting in a constant flow rate of 12.5 ml/min at a 5 V input.

The remaining blood can be stored in standard vials in the event that assays not currently performed on the analyzer are needed, or if the clinician decides that tests should be repeated to achieve a more reliable diagnosis.

C. Blood Analyzer Unit

The analyzer unit consists of the following components: a centrifuge to fractionate the blood sample, a microfluidic chip to house the sample, and an optical detection system to quantify the white cells and hematocrit.

1) Centrifuge: A miniaturized centrifuge (Fig. 2b) is used to spin the microfluidic chip at 10,000 rpm to separate the cellular components from plasma. The centrifuge is driven by a brushless servo motor (EC i-40, Maxon Motors) with an attached encoder to provide position and velocity control. Motor torque and power calculations governed the selection of the servo, assuming a required centrifugal force of 1,500 RCF for 5 min to fractionate the blood sample. Machined brackets are used to mount the motor to an aluminum base, which also serves as the mounting plate for the enclosure.

2) Microfluidic Chip: The single-use disposable chips house the blood sample and are fabricated using three layers of cast acrylic sheets which are laser cut and bonded into $\varnothing$72 mm chips. The top and bottom layers are 1.5 mm thick, whereas the middle layer is 0.8 mm thick. Plasma activation is used to enhance the wettability of the substrate, allowing the sample to easily flow into the channels once delivered from the peristaltic pump. The layers are bonded using pressure-sensitive adhesive and pressed together under 5 MPa of pressure at 65 ^{o}C for 5 min to ensure leak-proof channels. To differentially label nucleated white blood cells for imaging human samples, 5 μg of dry acridine orange fluorescent stain (A3568, Life Technologies) is pre-loaded in the chip during fabrication.

The use of centrifugal microfluidics minimizes the need for external pumping and complex valving mechanisms [13]. Specifically, the sample can be automatically manipulated on-chip by varying the speed of the centrifuge motor. The chip geometry consists of a wide inlet in the chip center and two parallel channels (3 mm wide) that curve back to the middle with pressure outlets at both ends. These parallel channels also serve as the detection chambers.

3) Optical Detection System: To image the blood sample, a miniaturized epi-fluoresecent microscope was developed for use with 475$\pm$35 nm excitation and 500$\pm$35 nm emission fluorophores (e.g. acridine orange). The system is mounted on two linear stages (LSM025 and LSA25, Zaber) to provide translation along y and z (denoted as y_o and z_o respectively in Fig. 2b). The components of the microscope include a high-powered blue LED (465–485 nm), excitation (475 $\pm$ 35 nm) and emission (500 nm high pass) filters, a dichroic mirror (506 nm), lenses (4x objective and f = 50 mm tube lens), and a CMOS sensor (FireFly MV, PointGrey) to capture the reflected light in an 8-bit grayscale image. The camera update rate is 30 fps for image capture and 20 fps for the subsequent processing.

After the centrifuge fractionates the sample, the motorized stages position the microscope over the fluorescing white cell region (also known as the buffy coat) using a pre-determined trajectory. The location in the y-dimension can be estimated from typical hematocrit levels (i.e. $\sim$45%) and the known sample volume, while the z_o-stage automatically translates upwards a set distance to get within focusing range. The z_o-stage then makes further adjustments to auto-focus the light by maximizing image contrast along the borders of the buffy coat (i.e. sharp transitions between the black background and white fluorescing region).

Once in focus, an image thresholding step is performed based on Otsu's method [14], and the thickness of the white cell region is quantified. The software then compares this measured thickness with pre-determined values to compute the total white cell count. Pre-determined values are obtained from generating a standard curve using samples with known cell concentrations. The standard curve is then converted to a look-up table in the software to rapidly output diagnostic cell

counts during run-time. To quantify hematocrit, the plasma volume is imaged by the microscope and converted to a %-volume, which is calculated based on the channel geometry and the sample volume in the chip.

D. Device Sterilization

Components of the device that come into contact with the patient must be sterilized or replaced as a disposable between uses. This includes the needle, US gel clip, and arm rest. Specifically, the needle and gel clip are packaged in a disposable cartridge and are inserted in the back of the device before each procedure. As described in [9], the robot positions the manipulator over the cartridge to load the needle and gel clip. After the venipuncture, both parts are automatically disposed in a sharps bin sitting beside the device. A disposable sheath wraps around the arm rest and is also replaced between uses; however in this case, the clinician manually places and removes it from the device.

During the needle insertion, there is minimal risk in blood contaminating other parts of the system such as the robotic and imaging components. The US gel clip, pressing against the patient's skin, serves to stabilize the vessel during the venipuncture and also prevents blood from contaminating the core components of the device. Finally, blood vials and the microfluidic disc need to be replaced between each use in the carousel and analyzer unit, respectively. Tubing from the peristaltic pump is cleaned after each procedure by flowing a saline wash fluid through the system.

III. Experimental Methods & Results

A series of *in vitro* experiments were conducted to evaluate each sub-system of the device. First, blood vessel phantoms were used to test the cannulation accuracy of the robot. Next, blood-mimicking fluid was used to test the automated sample handling module. Finally, human blood sample controls spiked with fluorescently labeled microbeads were used to test the analyzer unit.

A. Phantom Cannulations

Cannulation accuracy was first assessed in phantom models (Fig. 4), where a successful venipuncture was defined as placing the needle in the center of the surrogate vessel, and collection of 4 ml of fluid. Phantoms were fabricated based on the protocol described in [15], and extended by perfusing a viscous solution through the vessels. Briefly, phantoms contained two different sized veins (⌀3 and 2 mm) composed of silicone tubing (Silastic silicone, Dow-Corning) embedded in a 10% gelatin matrix. Blood-mimic fluid composed of 45% glycerol and water was then perfused through the surrogate veins at 35 ml/min using a syringe pump (representative of a standard flow rate found in adult forearm vessels).

1) Previous Work: Previous iterations of the device demonstrated close to 100% cannulation accuracy in gelatin phantom models [9]. However, in that study, the US probe was oriented longitudinally, and vessels tended to roll out of the US image if the needle was inserted off-axis. In [10], we rotated the US probe 90° to enable transverse imaging, and demonstrated how the device can adapt to rolling veins during the insertion via real-time visual servoing. However, we did not quantify the cannulation success rate of the system. Here, we perform a series of phantom cannulation experiments to assess the accuracy of the robot using transverse US-guidance. Furthermore, in these studies, successful cannulation was measured as the capacity to withdraw 4 ml of blood mimicking fluid from the vessels, as opposed to simply positioning the needle.

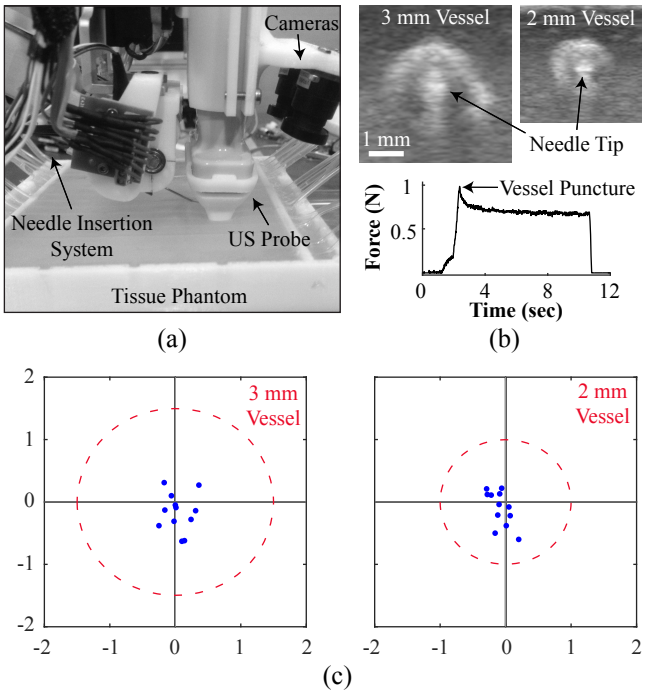

Fig. 4. Robotic cannulation testing. (a) Experimental set-up highlighting the needle manipulator and tissue phantom. (b) US images of the ⌀3 and 2 mm surrogate vessel during venipuncture trials, and corresponding force profile observed. (c) Robotic cannulation results (dotted red circle indicates vessel wall, blue dots indicate needle tip error for each trial; units in mm).

2) Experimental Protocol: The robot located the venipuncture site using the stereo cameras, oriented the end-effector along the vessel, and finally inserted the needle under US image and force guidance. In all trials, cannulation parameters were kept the same. Specifically, a 21 G needle was inserted at a constant 15° angle and a speed of 10 mm/s. The manipulator introduced the cannula into the phantom until a peak in the force profile was observed (as seen in Fig. 4b), confirming the vessel puncture. The robot then moved forward 5 mm along the x-axis and repeated this process a total of 6 times for each vein. Figure 4 displays the testing setup and cannulation results.

3) Results: The robot successfully placed the needle into the center of the vessel across all cannulation trials with a needle tip error of 0.3±0.2 mm and 0.3±0.1mm (mean ± s.d.) for the ⌀3 and 2 mm vein respectively. Here, positioning error was defined as the distance from the vessel center to the actual needle tip position (extracted from the US

TABLE I

FRACTIONAL FACTORIAL EXPERIMENTAL DESIGN USED TO EVALUATE SAMPLE COLLECTION TIME IN VACUTAINER BLOOD TUBES.

Parameter	Levels		
Needle size (G)	21	23	25
Vein OD (mm)	2	3	4.5
Viscosity (%)	35	45	55
Flow (ml/min)	35	45	55

image and registered to the robot coordinate frame). The subtle inaccuracies may have stemmed from errors in the joint kinematics, ultrasound calibration, or assembly of the system. Implementing a state estimation framework (e.g. Kalman filtering) to combine measurements from the US image, force sensor, and joint position sensors may improve the localization of the needle tip in future studies. Moreover, this could provide additional information, such as needle-tissue interaction along the vessel wall, to further enhance device safety.

B. Evaluation of the Sample Handling Module

Next, we performed a set of experiments to evaluate sample collection time in Vacutainer tubes. Similar blood vessel phantoms as previously described were used for experimental testing. In these trials, collection time was recorded over four variables—needle size, vein diameter, fluid viscosity, and flow rate—all consisting of three levels. A fractional factorial experimental design was implemented (4-variable, 3-level L9 orthogonal array [16]) to evaluate the effects of these variables on sample collection time. In total, 9 trials were conducted in triplicate, as outlined in Table I.

1) Experimental Protocol: After cannulating the phantom vessel, synchronized motions of z_{c1} and R of the blood collection carousel were used to dispense fluid into the Vacutainer tubes (Fig. 5a). These vials are evacuated and sealed with a rubber cap, enabling the vacuum to pull the indicated sample volume; in our case, 4 ml. The NIR sensor located on the carousel pump monitored tube volume levels throughout the experiments, allowing us to measure the time needed to fill the tubes.

2) Results: Analyzing the effect plots in Fig. 5b, the fill time increased with increasing fluid viscosities, suggesting that this parameter could potentially be used as a simple indicator of blood hematocrit in the sample and could also be used to tell the y_o-stage on the microscope precisely how far to translate to locate the buffy coat. At 35% glycerol concentration, it took 32.6 sec to fill the collection tubes, whereas for 55% concentration it took 70.9 sec.

Needle size affected sample collection time as well (24.2 versus 79.1 sec for 21 and 25 G needles respectively) with smaller gauge cannulas constricting fluid flow. This implies that smaller gauge needles should only be used when low sample volumes (i.e. $<$1 ml) are needed; otherwise the cannula risks being dislodged from the vessel due to the long time required for sample collection. Conversely, vein

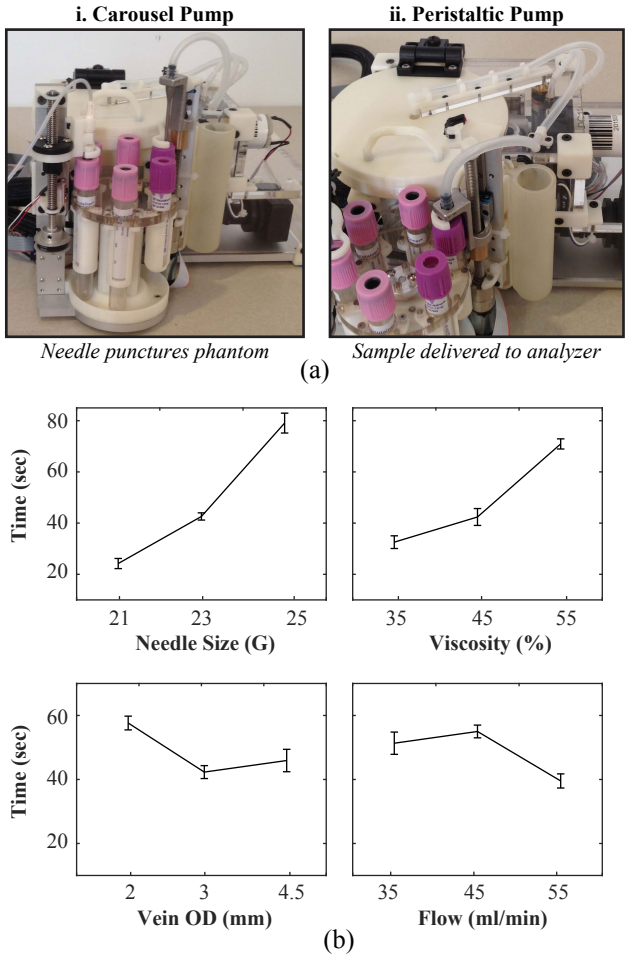

Fig. 5. Testing of the sample handling module. (a) Experimental setup of the sample collection study, highlighting the i. carousel pump and ii. peristaltic pump. (b) Effect plots for fractional factorial experimental design showing sample collection times for each variable and parameter. Data shown as mean $\pm$ s.d. for each level (n=3).

diameter and flow rate had minimal effect on collection time, possibly indicating that collection times may be similar among people with varying blood pressure levels. Finally, once the solution was collected, the peristaltic pump then delivered 200 μl of sample to the microfluidic chip.

C. Blood Analysis of Simulated Total White Cell Count

The last set of experiments demonstrated proof-of-concept of the blood analyzer using a simulated white cell assay, in which the area of the buffy coat was correlated with a cell count to generate a standard curve. We used *in vitro* human blood samples spiked with fluorescently labeled beads ($\varnothing$15 μm) to simulate white cells. The bead counts per μl of sample were 100, 200, and 300.

1) Experimental Protocol: First, 200 μl of sample was manually pipetted into the microfluidic chip and loaded into the analyzer unit. The centrifuge was then spun at 10,000 rpm for 5 min. Following centrifugation, the microscope auto-focused (z_o) and scanned the detection channel (y_o) for the fluorescing buffy coat. The y_o-stage translated until it found

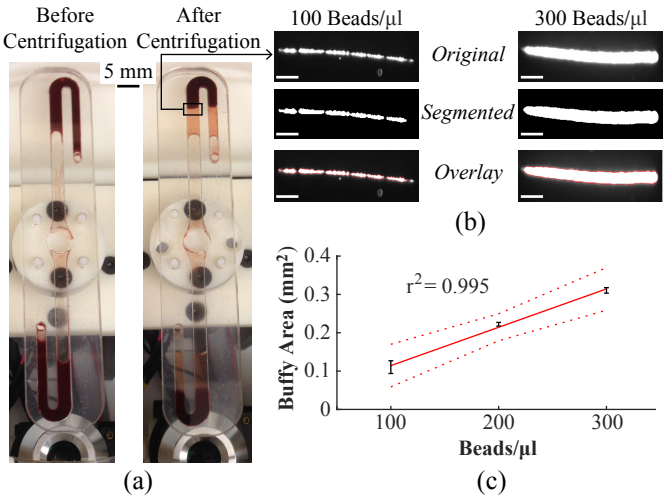

Fig. 6. Testing of the analyzer unit. (a) Chip before and after centrifugation. (b) Original and processed images of the buffy layer used to quantify the number of beads in the sample (scale bar = 0.5 mm for all images). (c) Standard curve for the bead-simulating white cell assay. Error bars show standard deviation for each level (n=3); red line shows the linear fit (r^2=0.995); dotted red lines show 90% confidence bounds.

the salient layer of packed beads, at which point a series of image processing steps were implemented to enhance, segment, and measure this region.

2) Results: The chip is displayed before and after centrifugation in Fig. 6a, and the image processing used to quantify the buffy coat area is shown in Fig. 6b. The standard curve (Fig. 6c), produced from plotting the measured buffy coat area with the known number of beads in each sample, resulted in a coefficient of variation of 0.995, indicating a near linear fit. The image processing algorithms were able to successfully segment and quantify the buffy coat for all trials. Standard deviations in the measured area (i.e. 15.10%, 2.16%, and 2.32% of the mean for 100, 200, and 300 beads/μl, respectively) were more likely due to inherent variations in manual sample preparation than to the segmentation algorithms.

However, there will likely be more variation in the segmentation results when testing with human samples. Specifically, stained white cells may not fluoresce as intensely as the microbeads used in this study, and this may introduce noise in the image processing. As an alternative method, we will investigate a summation of pixels approach to quantify the number of cells. Stained cells will appear as gray pixels in the image, while the background will be black. In future studies, we will produce a similar standard curve with blood samples of known white cell concentrations, and expand the plot to include a greater number of data points. This curve will be stored in the software as a look-up-table, in which the measured buffy coat is correlated to a cell count.

IV. Conclusion

In this paper, we presented the development of an automated blood draw and analysis device, and evaluated the system through a series of independent *in vitro* experiments. We investigated the cannulation accuracy of the venipuncture robot, sample collection time in the blood vials, and calibration parameters of the analyzer.

Future work includes conducting experiments on the fully integrated device to evaluate the system as a whole and comparing performance against manual blood testing approaches. Additionally, we would like to incorporate the detection of other blood parameters in the analyzer, such as large biomolecules and small metabolites. This would involve redesigning the microfluidic chip by modifying the channel geometries, as well as incorporating additional reagents.

Acknowledgment

This research was supported by the United States National Institutes of Health (R01EB020036). The work of M. Balter was supported by an NSF Graduate Research Fellowship (DGE-0937373). The work of A. Chen was supported by an NIH F31 Predoctoral Fellowship (EB018191).

References

[1] *The Freedonia Group, In vitro diagnostics in the U.S.*, 2011, vol. 59.
[2] J. Hammerling, "A review of medical errors in laboratory diagnostics and where we are today," *Lab. Med.*, vol. 43, no. 2, pp. 41–44, 2012.
[3] R. Niska, F. Bhuiya, and J. Xu, "National hospital ambulatory medical care survey: 2007 emergency department summary," *National Health Statistics Report*, pp. 1–31, 2010.
[4] G. Kost, Z. Tang, D. Shelby, and R. Louie, "Point-of-care testing: Millennium technology for critical care," *Lab. Med.*, vol. 31, no. 7, pp. 402–408, Jul 2000.
[5] C. Chin, V. Linder, and S. Sia, "Commercialization of microfluidic point-of-care diagnostic devices," *Lab chip*, vol. 12, no. 12, pp. 2118–34, Jun 2012.
[6] M. Bond and R. Richards-Kortum, "Drop-to-drop variation in the cellular components of fingerprick blood: Implications for point-of-care diagnostic development," *Am. J. Clin. Pathol.*, vol. 144, no. 6, pp. 885–894, 2015.
[7] C. Hawker, "Laboratory automation: Total and subtotal," *Clin. in Lab. Med.*, vol. 27, no. 4, pp. 749–770, 2007.
[8] A. Chen, M. Balter, T. Maguire, and M. Yarmush, "Real-time needle steering in response to rolling vein deformation by a 9-dof image-guided venipuncture robot," in *IEEE/RSJ Int. Conf. on Intelligent Robots and Systems*, 2015, pp. 2633–2638.
[9] M. Balter, A. Chen, T. Maguire, and M. Yarmush, "The system design and evaluation of a 7-dof image-guided venipuncture robot," *IEEE Trans. Robot*, vol. 31, no. 4, pp. 1044–1053, 2015.
[10] M. Balter, A. Chen, T. Maguire, and M. Yarmush, "Adaptive kinematic control of a robotic venipuncture device based on stereo vision, ultrasound, and force guidance," *IEEE Trans. Ind. Electron*, Forthcoming, 2016.
[11] A. Osei-Bimpong, R. McLean, E. Bhonda, and S. Lewis, "The use of the white cell count and haemoglobin in combination as an effective screen to predict the normality of the full blood count." *Int. J. of Lab. Hematol.*, vol. 34, no. 1, pp. 91–7, 2012.
[12] R. Brewer, "Improving peripheral iv catheterization through robotics: From simple assistive devices to a fully-autonomous system," Doctor of Philosophy, Stanford University, 2015.
[13] R. Gorkin, J. Park, J. Siegrist, M. Amasia, B. Lee, J. Park, J. Kim, H. Kim, M. Madou, and Y. Cho, "Centrifugal microfluidics for biomedical applications," *Lab Chip*, vol. 10, no. 14, pp. 1758–73, 2010.
[14] N. Otsu, "A threshold selection method from gray-level histograms," *IEEE Trans. Syst., Man, Cybern., Syst*, vol. 20, no. 1, pp. 62–66, 1979.
[15] A. Chen, M. Balter, M. Chen, D. Gross, S. Alam, T. Maguire, and M. Yarmush, "Multilayered tissue mimicking skin and vessel phantoms with tunable mechanical, optical, and acoustic properties," *Med. Phys.*, vol. 43, no. 6, pp. 3117–3131, 2016.
[16] J. Antony and M. Kaye, "Methodology for taguchi design of experiments for continuous quality improvement," *Quality World*, pp. 98–102, 1995.